Tribology International 192 (2024) 109335

Contents lists available at ScienceDirect

Tribology International

journal homepage: www.elsevier.com/locate/triboint

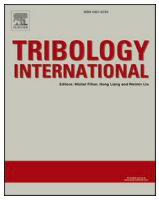

Coating sensing strategy for understanding the governing factors of tribofilm growth on diamond-like carbon

Nan Xu *, Chun Wang, Dongze Wang, Liuquan Yang, Ardian Morina

Institute of Functional Surfaces, School of Mechanical Engineering, University of Leeds, Leeds LS2 9JT, United Kingdom

ARTICLE INFO

Keywords:
Tribo-chemistry
Tribofilm growth
Additive
Raman
Diamond-like carbon
in-situ identification

ABSTRACT

Tribofilms formed on coating surface can replace the original surface materials and dominate the final tribological behaviors. *In-situ* identification techniques of additive-derived tribofilm significantly contribute to understanding the tribo-chemical reaction mechanisms between additives and coatings. Here, a Raman-based profilometry was employed for in-situ identifying tribo-chemical products formed on a-C:H surface based on their distinct optical properties. By combining diverse characterization techniques, the effectiveness of Raman-based method was verified, and a surface-dependent tribofilm growth mechanism was proposed. It is suggested that the tribo-chemical reaction between additive-derived tribo-products and a-C:H is mainly governed by the Lewis acid-base property of coating surface under low contact pressure and temperature condition, highlighting the critical role of chemical property of coating surface in initiating tribofilm growth.

1. Introduction

Advanced coating techniques have been increasingly applied in a wide range of engineering applications, including manufacturing, vehicles, and aeronautics [1–4]. In combination with liquid lubricants, the protective coatings on key mechanical components can dramatically reduce the friction and extend the service life by orders of magnitude, leading to considerable materials and energy savings [5,6]. Additives are the crucial components of liquid lubricants and their tribo-chemical products formed on coating surfaces (tribofilm) critically affect the wear and friction behaviors. Deepening the understanding of the growth mechanisms of additive-derived tribofilm on coating surfaces can significantly contribute to developing effective lubricating solutions for diverse coating materials. However, the mechanisms governing the tribofilm growth on coating surfaces are not well understood since most of existing lubricating additives are developed for ferrous surfaces [7–11]. An inappropriate use of lubricating additives can result in severe wear and early failure of surface functional coatings. For example, when using the traditional friction modifier MoDTC, which is designed for ferrous-based surfaces, MoDTC-derived products can cause dramatical wear acceleration on diamond-like carbon coatings (DLC) [12–15].

In the past decades, a significant progress has been achieved in identifying the structure and composition of additive-derived tribofilm via advanced surface analysis techniques. Particular attention is paid on the governing factors in the tribofilm growth of ZDDP which is one of the most crucial anti-wear additives, highlighting the activation effect of pressure and temperature in the tribochemical reactions [16–18]. As indicated in the literature, despite employing DLC coatings with different chemical structure (e.g., hydrogen content and sp^2/sp^3 ratio) and mechanical properties, the growth process of ZDDP tribofilm is dominated by effective local contact pressure rather than the chemical structure of coatings [19]. However, it is interesting to note that the tribofilms formed on DLC surface are less durable than those formed on ferrous surfaces [20,21]. Meanwhile, based on the results of surface element analysis on ferrous and DLC surfaces, it is found that ZDDP tribofilms prefer to form on the ferrous surface rather than on DLC [22,23]. Although the reasons for this surface-dependent growth remain unknown, these findings clearly confirm the critical role of surface materials in the tribofilm growth process. Substantial efforts should be made to classify which key characteristics of surface materials govern the tribofilm growth and their final mechanical properties (e.g., wear resistance and load carrying capacity) since it directly determines the basic concepts in designing effectively lubricating solutions for diverse surface materials.

As indicated in the literature, the growth process of ZDDP-derived tribofilm includes three stages, including nucleation (initial stage), growth, and thickness saturation [16]. ZDDP can form surface-bonded pad-like tribofilms of a gradient structure, with a short-chain glassy

* Corresponding author.
E-mail address: n.xu@leeds.ac.uk (N. Xu).

https://doi.org/10.1016/j.triboint.2024.109335
Received 3 January 2024; Received in revised form 20 January 2024; Accepted 22 January 2024
Available online 24 January 2024

phosphate near the ferrous surface and a thin outer layer of long-chain polyphosphates [17,18]. It is well accepted that the governing factors of ZDDP tribofilm formation in the growth and thickness saturation stages are stress and temperature [16–18], while there is considerable disagreement on the governing factors in the initial stage. Some studies indicated that the nucleation stage (initial stage) of ZDDP tribofilm on steel surface should stem from the Lewis acid-base interaction between ZDDP-derived phosphate and oxidized ferrous surface [17,24–27]. Specifically, Fe^{3+} is hard Lewis acid (electron-pair acceptor) and prefers to react with phosphate of hard Lewis base (electron pair donor), according to the hard and soft acids and bases principle (HSAB). However, there is no general consensus on the dominating role of Lewis acid-base interaction in tribofilm growth due to lacking direct experiment evidence.

In our previous study, a highly accurate Raman-based profilometry is employed to quantify the thickness of a-C:H coatings based on the Raman signal intensity [28]. Since this proposed method is sensitive to the variation of surface optical properties, it is used in this study to identify the additive-derived tribofilms formed on a-C:H, based on the different optical properties of diverse tribochemical products. Specifically, MoDTC-derived products (e.g., MoS_2 and MoC) with lower transmittance (higher absorption coefficient or/and reflectivity than a-C:H) towards Raman signal can cause extra attenuation of Raman intensity and consequently, remarkable measurement deviations of a-C:H [29], whereas the glassy tribofilms derived from ZDDP hardly affect the Raman intensity due to their high transmittance [30,31] and accurate a-C:H thickness can be obtained. It is found that under low contact pressure and temperature conditions, ZDDP-derived tribofilms can form on a-C:H surfaces when using ZDDP in combination with MoDTC. In the case of using a model oil with only ZDDP, no ZDDP tribofilm was detected on a-C:H. By combining detailed structural and composition analysis towards the contact surface, an obvious oxidized a-C:H surface layer was observed, which can transform the contact surface from Lewis base (a-C:H) to Lewis acid (oxidized a-C:H) and play a dominating role in the selective growth of ZDDP tribofilms (Lewis base) based on HSAB principle. The formation of oxidation layer is attributed to the catalytic oxidation effect of MoDTC-derived molybdenum oxides towards a-C:H surface. This study directly demonstrates the critical role of Lewis acid-base interaction in the ZDDP tribofilm growth and provide a new pathway for identifying the tribochemical products, which can benefit the understanding of tribochemical interaction between coating and lubricants, and the design of novel solid-liquid lubricants.

2. Experimental method

2.1. Synthesis of a-C:H coatings

The a-C:H was deposited by a Plasma Enhanced Chemical Vapor Deposition technique (PECVD) with acetylene as gas feed (Flexicoat 850, Hauzer Corp., Netherlands). Detailed deposition parameters were shown in our previous studies [28,29]. Table S1 gives the optical and mechanical properties of a-C:H.

2.2. Tribological experiments

The friction experiments were conducted on a-C:H coatings deposited on silicon wafer with a fixed upper ball as the counterpart (AISI 52100 steel, 6.35 mm in diameter, HRC 60–67) by using ball-on-disc tribometer (Bruker UMT-Tribolab) at room temperature under oil-lubricated condition. A polyalphaolefin (PAO) base oil with different additives (PAO4 +0.8 wt% ZDDP, PAO4 +0.8 wt% MoDTC, PAO4 +0.8 wt% ZDDP + 0.4–1.2 wt% MoDTC) was used for the tribological tests. Here, secondary ZDDP is used in the test. Tribo-test conditions were testing time of 30 to 140 mins, applied load of 1 N to 30 N, speed of 10 mm/s, 20 ℃, and ambient environment. Here, tribotests were designed for investigating the impact of load and time on tribofilm growth. Three tests were conducted under the same test condition to verify the repeatability.

2.3. Materials characterization

Renishaw inVia™ Raman spectrometer was applied to measure the a-C:H thickness in the line-scanning mode and backscattering geometry, with 488 nm laser and 1 mW laser power. Before using NPFLEX 3D non-contact optical profilometer to characterize the wear scars, an iridium layer was deposited on the tribo-tested samples to avoid measurement errors caused by tribo-induced effect and tribofilm formation on coating surfaces [28,29].

A focused ion beam (FIB, FEI Helios G4 CX DualBeam FIB-SEM) was used to prepare thin cross-sectional lamellar specimens for TEM (transmission electron microscopy) investigations. FEI Titan3 Themis 300 TEM/STEM (Scanning transmission electron microscopy) equipped with Gatan Quantum ER energy filter and energy dispersive X-ray spectroscopy (EDS) was employed for TEM characterization, elemental analysis, and electron energy loss spectroscopy (EELS). HAADF (high-angle annular dark-field) image was acquired in the STEM mode. Note that EELS in STEM mode could provide detailed information of bonding structure in the atomic resolution. Gaussian peak fitting was adopted to quantify the bonding fractions. Detailed information of preparing FIB samples and Gaussian peak fitting was given in our previous studies [28].

3. Results and discussion

3.1. Selective growth of additive-derived tribofilms on a-C:H surfaces

As shown in Fig. 1, tribo-tests were conducted on a-C:H/steel contact under additive-lubricated condition with load of 1 N. When MoDTC is introduced into the lubricating oil with ZDDP as additive, the friction-reducing property is improved significantly with friction coefficient reduced from 0.12 to 0.07, which is close to the condition with only MoDTC as additive. When using ZDDP as additive, the wear only takes place on the steel ball and the ZDDP-derived tribofilm could only be observed on the surface of steel ball rather on a-C:H (Fig. 1B and C). For the condition of MoDTC (Fig. 1B and G), no tribofilm is observed on a-C:H and the main reason of triggering the dramatical wear on both a-C:H and steel is attributed to abrasive wear induced by MoDTC-derived tribo-products [29]. Here, the interesting finding is that the combination of MoDTC and ZDDP can significantly promote tribofilm growth on a-C:H surface with only slight wear. With increasing the MoDTC concentration from 0 to 1.2 wt%, the coverage rate of tribofilms on DLC surface increases obviously as shown in Fig. 1C-F. To gain fundamental insights into the mechanisms of tribofilm growth on coating surface and the synergistic effect in improving antiwear and friction-reducing properties, a Raman-based profilometry is employed to identify the tribofilm compositions in the later section.

3.2. Identification of additive-derived tribofilm by Raman-based profilometry

A highly sensitive Raman-based profilometry is employed here to identify the additive-derived tribofilm formed on a-C:H. As demonstrated in our previous study [28], this proposed method could provide accurate wear depth of a-C:H based on the Raman signal intensity from silicon sensing underlayer. However, the formation of additive-derived tribofilm on coating surfaces can cause obvious measurement deviations of wear depth, which can be used to provide key information of tribofilm compositions based on their known optical properties [29].

As shown in Fig. 2, a series of tribo-tests with different test time were conducted under oil lubrication (PAO4 +0.8 wt% ZDDP + 0.8 wt% MoDTC). After removing the lubricating oil with heptane, Raman spectroscopy under the line-scanning mode was employed to detect the

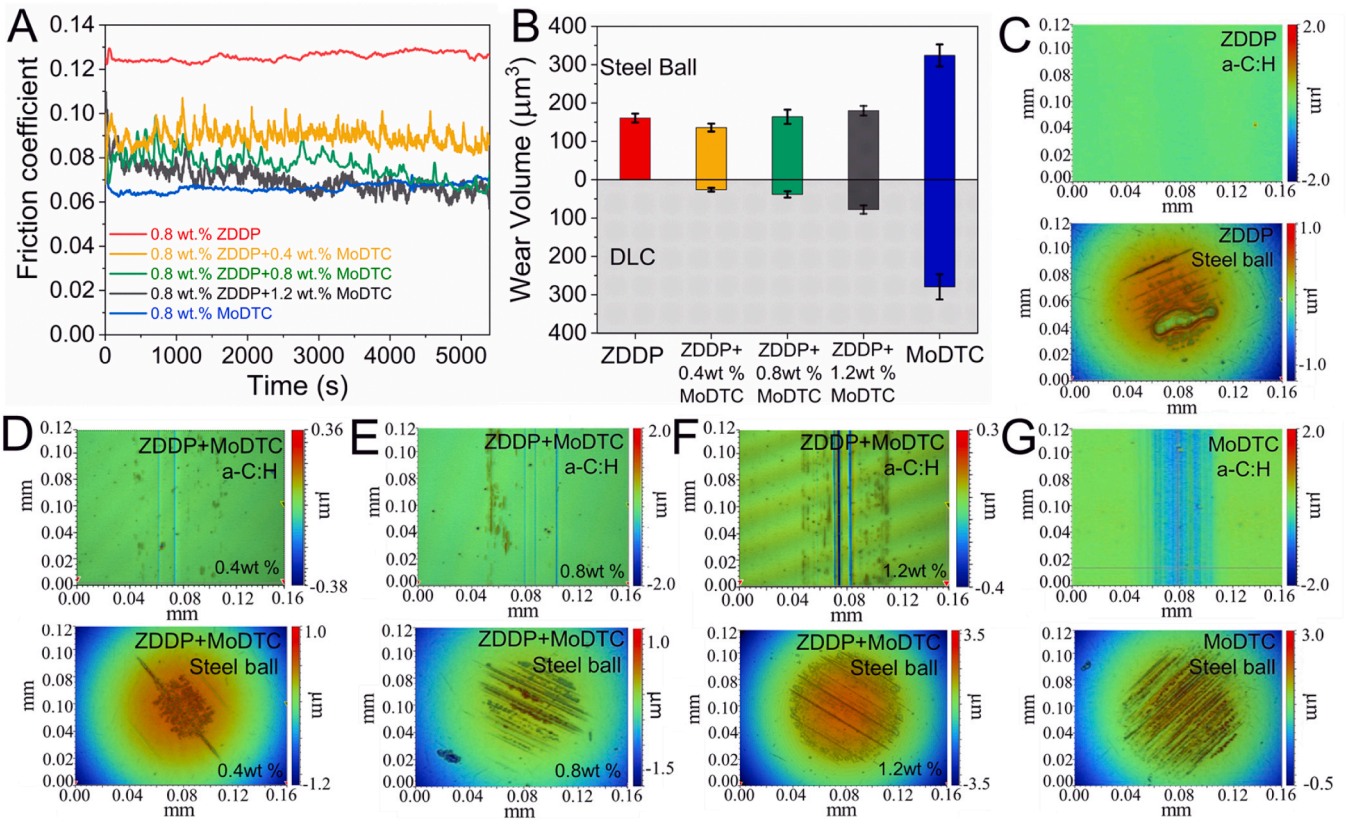

Fig. 1. Friction and wear behaviors of a-C:H coatings under oil lubrication (test condition: 1 N, 90 mins). (A) Friction coefficient curves. (B) Wear volumes on steel ball and DLC coatings obtained by optical profilometer. (C-G) The corresponding 3D optical microscopic images of wear scars on steel ball and DLC coatings (C, PAO4 +0.8 wt% ZDDP; D, PAO4 +0.8 wt% ZDDP + 0.4 wt% MoDTC; E, PAO4 +0.8 wt% ZDDP + 0.8 wt% MoDTC; F, PAO4 +0.8 wt% ZDDP + 1.2 wt% MoDTC; G, PAO4 +0.8 wt% MoDTC).

Raman signal intensity from silicon sensing underlayer across the wear scars, as shown in Fig. 2A-D. The top a-C:H thickness can be calculated based on the Raman signal intensity by the equation [28,29]:

$$t = -\frac{1}{\alpha_o + \alpha_1}\ln\frac{I_s}{I_o\beta(1-R_o)^2(1-R_1)^2} = \frac{-1}{\alpha_o + \alpha_1}\left[\ln I_s - \ln I_o\beta - \ln(1-R_o)^2(1-R_1)^2\right] \quad (1)$$

where t is the thickness (unit: μm), β is light scattering rate, $I_o\beta$ is Raman intensity of silicon 1st band of silicon substrate, R_o and α_o are the reflectivity and absorption coefficient of a-C:H for incident light, and R_1 and α_1 are that for scattered light. Detailed information can be found in S1section (supporting information).

Non-contact optical profilometer was then employed to characterize the wear scars along the same traces of Raman line-scanning (marked as dot lines in Fig. 2E-H). Note that, the tribofilms of different optical properties with a-C:H coating can result in obvious measurement errors for optical profilometer [29]. For obtaining accurate wear depth, optical profilometer is used after depositing iridium layer of uniform thickness (ca. 20 nm) on a-C:H surface (Fig. S1), as the top iridium layer can provide a test surface with same optical properties [28,29]. The results obtained by optical profilometer are then employed as standard reference for the coating thickness or wear depth [29]. By comparing the wear profiles obtained by Raman-based method and optical profilometer in Fig. 2I-L, it is interesting to find that on the positions with tribofilm formation, optical profilometer detects obvious depth-rising regions, while these regions cannot be detected by the Raman-based method.

To further verify the actual coating thickness, FIB technique was employed to fabricate cross-sectional lamellar specimen on a-C:H coating surface as marked in Fig. 2K. Two windows were obtained by FIB as shown in Fig. 3A. Windows 1 and 2 correspond to the surface areas with and without tribofilm, respectively. The corresponding TEM images were given in Fig. 3B-D. Through comparison, it is found that the coating thicknesses in the two areas are ca. 276 nm which is same with the thickness of synthesized a-C:H coating (Table S1), agreeing with the results obtained by Raman-based method in Fig. 2K. It is therefore suggested that the measured depth difference between Raman-based method and optical profilometer is caused by the tribofilm formation.

This finding raises an important question why Raman-based method cannot detect the tribofilm thickness. As illustrated in Fig. 4, this proposed method can identify the tribofilms based on their transmittance towards Raman laser. Here, the transmittance is determined by the absorption coefficient and reflectivity [28,29]. Tribofilm composed of tribochemical products with low transmittance towards Raman laser can cause extra attenuation of Raman signal intensity ($I_L < I_S$). Since the reduction in Raman signal corresponds to the thickening of coating, it can result in remarkable measurement deviations of a-C:H thickness in the form of wear depth rising compared with the depth reference from optical profilometer [29]. In contrast, the tribofilm with high transmittance can hardly be detected due to the negligible attenuation towards Raman signal intensity ($I_H \approx I_S$) and accurate coating thickness can be obtained. Based on this deduction, the tribofilm formed on a-C:H in Fig. 2 should be composed of materials with high transmittance. As reported in the previous studies [12–14], the main degradation products of MoDTC in friction process are MoC, MoO_3 and MoS_2, which display low transmittance towards Raman laser (488 nm). The main components of ZDDP-derived tribofilm are short-chain glassy phosphate and long-chain polyphosphates with high transmittance [17,18,30,31]. Therefore, based on the measurement principle of Raman-based

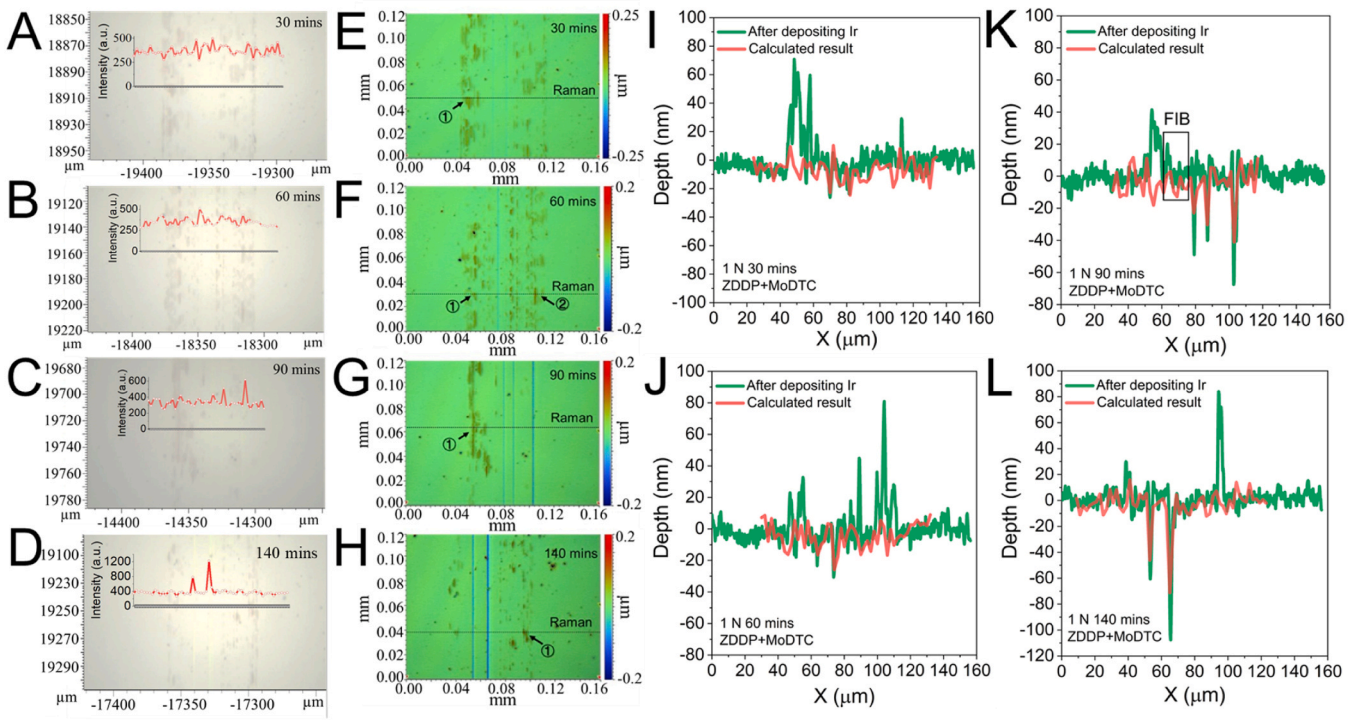

Fig. 2. *In-situ* identification of additive-derived tribofilms. (A-D) Optical images of line-scanning trace of Raman spectroscopy across the wear scars under different test time (oil lubrication: PAO + 0.8 wt%ZDDP+0.8 wt% MoDTC) and the corresponding Raman intensity of silicon signals which are used to quantify the a-C:H thickness. (E-H) 3D optical microscopic images of wear scars under different test time. The dot lines marked the line-scanning trace of Raman spectroscopy. (I-L) Comparison between wear profiles obtained by Raman-based profilometry and non-contact optical profilometer along the same traces. FIB test position is marked in K.

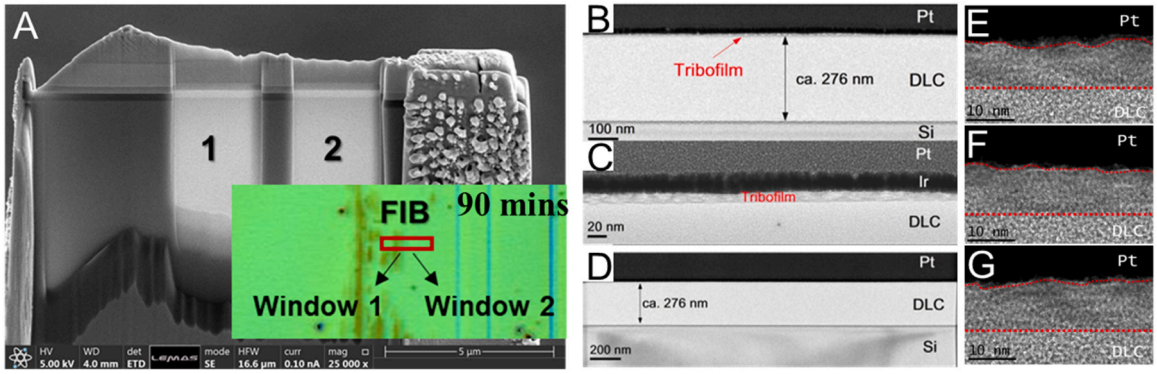

Fig. 3. *In-situ* observation of tribofilm and coating thickness. (A) SEM image of cross-sectional lamellar specimen as marked in Fig. 2K fabricated by FIB (window 1 with tribofilm and window 2 without tribofilm). The insert shows the FIB position on the tribo-tested sample in Fig. 2G and K. (B) TEM image showing the coating surface with tribofilm in window 1. (C) TEM image showing the tribofilm as marked in (B). (D) TEM image showing the area without tribofilm in window 2. (E-F) HRTEM images showing the tribofilm microstructure.

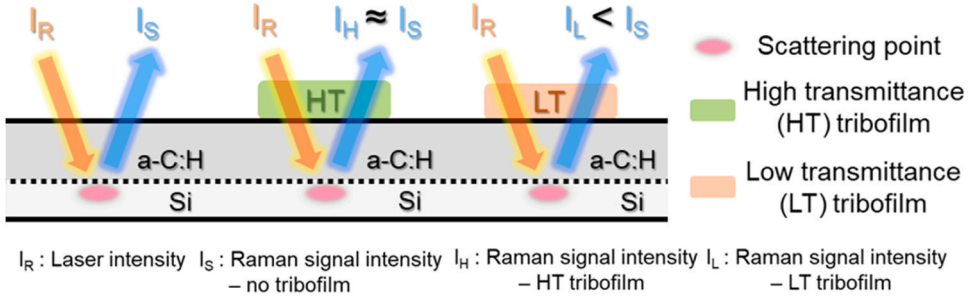

Fig. 4. Schematic illustration of Raman-based method in identifying the additive-derived tribofilm on coating surface.

profilometry and the optical properties of the above tribochemical products, the main tribofilm component should be glassy ZDDP-derived phosphates rather than MoDTC-derived products, agreeing with the tribofilm microstructures observed in the TEM images (Fig. 3E-G).

To further verify the tribofilm composition in Fig. 3C (PAO + 0.8 wt % ZDDP+0.8 wt% MoDTC), the FIB cross-sectional lamellar specimen of a-C:H coating was investigated by TEM and EDX. Fig. 5A shows a high-angle annular dark-field (HAADF) image of the cross-section of tribofilm area on a-C:H surface, with the EDX line-scanning trace. In Fig. 5B and C, the presence of elements P, Zn and O in the tribofilm is confirmed by EDX mapping and line-scanning along the trace as marked in Fig. 5A. Given the low content of element Mo, the element S should mainly result from the partial substitution for O element in the chain backbone of phosphate rather than MoDTC-derived MoS_2 [17,29]. Therefore, the main component of tribofilm should be zinc phosphate, agreeing with the above deduction based on Raman-based profilometry.

For further verifying the high sensitivity of this proposed Raman-based profilometry towards tribochemical products, this method is used to characterize the tribo-tested samples with MoDTC as additives, as shown in Fig. 6A (1 N, 30 mins). Fig. 6B displays the results of Raman line-scanning test across the wear scar. It can be observed that the characteristic peaks of MoS_2 at 385 cm^{-1} and 410 cm^{-1} cannot be detected due to the small crystal size of MoS_2. However, the proposed Raman-based profilometry can give useful information for identifying nano-MoS_2. As shown in Fig. 6C, the proposed approach is employed to characterize the tribo-tested sample based on the Raman signal intensity of silicon sensing underlayer. The significant mismatch between the wear profiles obtained by optical profilometer and Raman profilometry can be observed. It indicated the formation of tribofilm with low transmittance, according to principle in Fig. 4. As MoS_2 possessed lower transmittance (higher absorption coefficient or/and reflectivity) than a-C:H coating [29], it is suggested that MoS_2 should be the main tribochemical products of MoDTC. FIB technique is then employed to fabricate cross-sectional lamellar specimen on marked point in Fig. 6C and the corresponding HRTEM images are given in Fig. 6D and E. It can be observed that MoS_2 with crystal size of ca. 5 nm was formed on coating surface, demonstrating the high sensitivity of Raman-based profilometry.

3.3. Governing factor in the growth of additive-derived tribofilm

As shown in Fig. 1, the comparation tests with different additives were conducted under the same test condition (1 N, 10 mm/s, 20 °C). The formation of ZDDP-derived tribofilm was only observed on a-C:H surface when combining MoDTC with ZDDP as additives, while no ZDDP-derived tribofilm was formed when ZDDP was used alone as additive. Meanwhile, the coverage rate of ZDDP-derived tribofilms on a-C:H surfaces increased notably with MoDTC concentration (Fig. 1C-F). Deeply understanding the tribofilm growth can benefit the development of effective lubricating solution for diverse coating materials.

As indicated in the introduction, the tribofilm growth process is mainly controlled by applied stress, temperature and the physico-chemical properties of surface materials. To clarify the impact of stress on ZDDP tribofilm growth, the surface roughness should be considered, in view of that the increase of surface roughness on contact surface can result in the reduction of real contact area (A) [32–34] and the increase of contact pressure and shear stress. As shown in Fig. S2 (supporting information), the real contact areas under different surface roughness were given and the detailed information of calculation method can be found in section S1.2. Table 1 lists the surface roughness and the corresponding contact areas of tribo-tested samples with same test conditions and different additives. Here, the surface roughness value $R_q^{ball+DLC}$ ($R_q^{ball} + R_q^{DLC}$) is used in the calculation of real contact area. The surface roughness of tribo-tested samples with ZDDP as additive displayed higher value than that with ZDDP+MoDTC as additives, resulting in reduced contact area and increased contact pressure. In addition, in view of the high friction coefficient (high shear force) and reduced real contact area (high surface roughness) when using ZDDP as additive, the

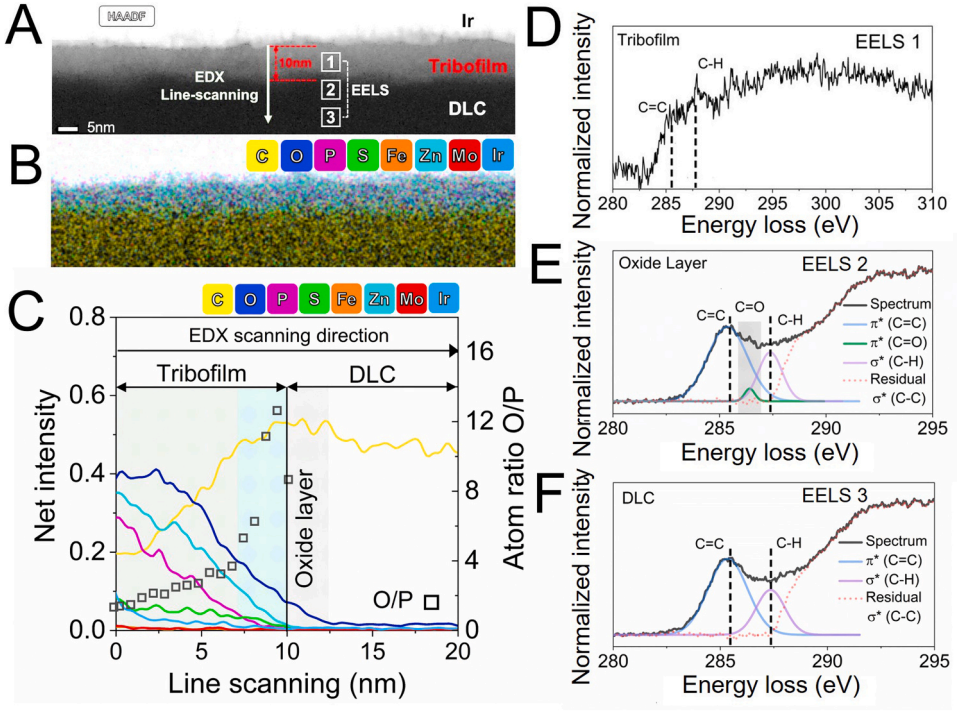

Fig. 5. Characterization on the tribofilm composition in Fig. 3C (PAO + 0.8 wt% ZDDP+0.8 wt% MoDTC). (A) HAADF image from area with tribofilm formation on a-C:H surface showing the EDX line-scanning trace and EELS test positions. (B) EDX mapping image. (C) EDX line-scanning profile along the trace as marked in (A) and atomic ratio of oxygen element to phosphorus element in tribofilm. (D-F) EELS Carbon K-edge spectra in three regions of the cross-section of a-C:H (D, tribofilm; E, oxidized a-C:H layer; F, a-C:H sublayer). The residual bond fraction is assigned to σ * (C-C, sp^3).

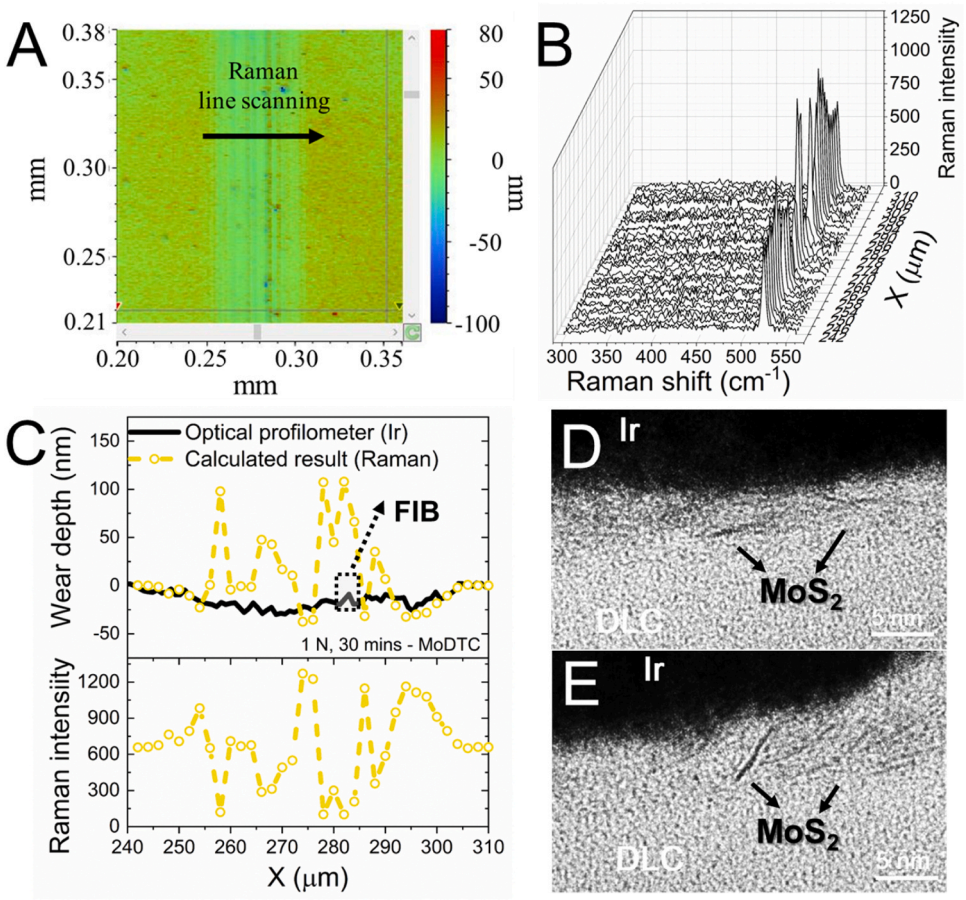

Fig. 6. (A) 3D optical microscopic images of wear scar with the line-scanning trace of Raman test (PAO4 +0.8 wt% MoDTC; test condition: 1 N, 30 mins). (B) Raman spectra obtained from line-scanning. (C) Wear profiles obtained from optical profilometer and Raman-based profilometry, and Raman intensities of silicon bands from silicon sensing underlayer obtained by Raman line-scanning in (B). (D and E) HRTEM images showing the tribofilms with nano-MoS_2 sheet on the marked area in (C).

Table 1
Surface roughness values (R_q), real contact area (A), contact pressure (P), and shear stress (τ) on contact surfaces shown in Fig. 1C-G.

Samples	0.8 wt% ZDDP	0.8 wt% ZDDP 0.4 wt% MoDTC	0.8 wt% ZDDP 0.8 wt% MoDTC	0.8 wt% ZDDP 1.2 wt% MoDTC	0.8 wt% MoDTC
R_q^{Ball}	89.3 nm	53.9 nm	57.6 nm	63.7 nm	98.5 nm
R_q^{DLC}	7.2 nm	9.5 nm	11.7 nm	15.8 nm	52.7 nm
$R_q^{Ball+DLC}$	96.5 nm	63.4 nm	69.3 nm	79.5 nm	151.2 nm
A (μm^2)	227	334	306	273	149
P (GPa)	4.4	2.9	3.2	3.7	6.7
μ	0.126	0.093	0.078	0.072	0.062
F_S (N)	0.126	0.093	0.078	0.072	0.062
τ (GPa)	0.56	0.28	0.25	0.26	0.42

Test conditions: 1 N, 90 mins, 20 ℃. R_q of steel ball surface before tribo-test: ca. 10 nm. R_q of DLC coating surface before tribo-test: ca. 6 nm. R_q is measured by optical profilometer. A is real contact area. P is contact pressure. μ is friction coefficient. F_S (shear force or friction force) = $\mu \cdot F_N$. F_N is normal force (1 N). τ (shear stress) = F_S / A.

corresponding shear stress exceeded that with ZDDP+MoDTC as additives, as displayed in Table 1. According to the literature [16–19], increasing applied stress (contact pressure and shear stress) can promote the tribofilm growth based on stress-dependent mechanism. However, there was no ZDDP tribofilm formed under the higher stress condition with only ZDDP as additive. Meanwhile, the test temperature of 20 ℃ cannot activate the growth of ZDDP-derived tribofilm. As reported in the previous study [16], the growth rate of ZDDP tribofilm kept at very low level even under the condition of 4.4 GPa and 80 ℃. It is therefore suggested that the applied stress and temperature are not the main governing factors of ZDDP tribofilm growth under current test conditions.

Since the ZDDP tribofilm has displayed a characteristic of surface-dependent growth [20–23], EDX and EELS were employed to investigate the composition of interface between tribofilm and coating surface for further clarifying the governing factor of ZDDP tribofilm growth on a-C:H. An interesting finding is the existence of oxide layer with thickness of 2.5 nm on the a-C:H surface, as displayed in the EDX line-scanning analysis (Fig. 5C). Meanwhile, the atomic ratio of oxygen to phosphorus (O/P ratio) is given and shows a declining trend from the bottom to the top of tribofilm. This agrees with the gradient structure of ZDDP tribofilm, which is composited of a short-chain glassy phosphate with high O/P ratio on the bottom and a thin outer layer of long-chain polyphosphate with low O/P ratio [17,18].

In addition, analyses on EELS carbon K-edge spectra were carried out for investigating the bonding composition of sp^2 (1 s-to-π *) and sp^3 (1 s-to-σ *) in three different areas, including tribofilm, oxidized a-C:H layer and a-C:H sublayer. Typically, the peak centers of 1 s-to-π * and 1 s-to-σ * transitions locate in the regions of 284 to 287 eV and 287 to 310 eV, respectively [35,36]. As shown in Fig. 5D, the main bonding structure of ZDDP-derived tribofilm is sp^3, agreeing with chemical composition (C-C bonds) of ZDDP and base oil. Fig. 5E and F present the EELS spectra collected from oxidized layer and sublayer of a-C:H. Gaussian peaks fitting were adopted to investigate the bonding composition, as shown in Fig. S3. The typical peaks of C═C (sp^2,

1 s-to-π *) and C-H (sp^3, 1 s-to-σ *), centered at 285.5 and 287.5 eV [37,38], have been well defined in the EELS spectra. There is a notable mismatch area when two Gaussian peaks fitting was used to analysis the EELS spectra of oxidized a-C:H layer in Fig. S3B, while no such area was observed on that of non-oxidized a-C:H sublayer in Fig. S3D. To further clarify the bonding composition, analyses involving three Gaussian peaks fitting were conducted in Fig. S3A and C, which are also displayed in Fig. 5E and F, respectively. It can be observed that the additional peak, corresponding to the mismatch area, appears on the high-energy side of C═C peak in the EELS spectrum of oxidized a-C:H layer (gray area in Fig. 5E), which cannot be observed in the spectrum of a-C:H sublayer (Fig. 5F). Since this peak is caused by the oxidation of a-C:H and the peak center at 286.5 eV is in the region of sp^2 (1 s-to-π *), it is suggested that this feature peak belongs to C═O (sp^2, 1 s-to-π *) [38,39]. In addition, the bonding fractions were calculated based on the peak areas and shown in Table 2. Detailed information of calculation process can be found in our previous studies [28,29]. The sp^2 and sp^3 fractions in oxidized layer of a-C:H are 63.2% and 36.8%, while that in the a-C:H sublayer are 60.2% and 39.8%. Therefore, the oxidized layer underwent a bonding transformation from sp^3 to sp^2, which is about 3% and close to the C═O fraction (2.6%). It indicates that the oxidation of carbon in a-C:H prompts the bond dissociation of C-C and C-H, and transformation from sp^3 to sp^2.

The oxidized site with C═O group possesses Lewis acid property [40,41], which transforms a-C:H surface from Lewis base to Lewis acid. Based on the Lewis acid-base interaction [42–44], the absorption of ZDDP-derived phosphate (Lewis base) on the oxidized a-C:H surface can be effectively promoted. Meanwhile, since the Lewis acid centers with C═O groups preferably react with nucleophiles [45,46], it provides active sites to initiate the tribochemical reaction with ZDDP-derived phosphate, further promoting the growth of ZDDP tribofilm. As indicated in previous work [47,48], the synthesized a-C:H surfaces can readily get oxidized after exposure to ambient air. However, this kind of oxidized layer with thickness less than 1 nm is completely removed after the initial running-in process. To obtain stable replenishment of ZDDP tribofilms on coating surface, the continuous existence of oxidized layer on coating surface is necessary. As shown Fig. 1, increasing the MoDTC concentration can dramatically increase the coverage rate of tribofilm, indicating the key role of MoDTC in the formation of ZDDP tribofilm on a-C:H surfaces. Meanwhile, it has been well demonstrated that MoDTC will degrade into MoS_2 and MoO_3 in the friction process [13–15,29,49,50] and MoO_3 is a typical catalyst to promote the oxidation of carbon materials (e.g., carbon black and soot) [29,51–56]. In addition, the element composition on the surface of tribo-tested a-C:H with only ZDDP as additive was also investigated by EDX line-scanning and there is no oxidized DLC layer observed on DLC coating surface, as shown in Fig. 7. It is therefore suggested that the stable oxidized layer on coating surface is introduced by the continuously catalytic oxidation of MoDTC-derived MoO_3 towards the a-C:H surface. It should be also pointed out that ZDDP cannot prevent the a-C:H oxidation induced by MoO_3. This is because the oxidation inhibition mechanism of ZDDP towards lubricating oil is that it acts as peroxide decomposer and radical scavenger in the oxidation process of lubricating oil, which is different from the oxidation mechanism of MoO_3 to a-C:H. Based on the above results, it is therefore suggested that the Lewis acid-base interaction plays a crucial role in the growth of ZDDP tribofilm on a-C:H surface under low applied stress and temperature.

Table 2
EELS C-bonds fractions of oxidized layer and sublayer of a-C:H.

Region	sp^2		sp^3	
	C═C	C═O	C-H	C-C
Oxidized a-C:H layer	60.6%	2.6%	23.9%	12.9%
Sublayer (a-C:H)	60.2%	-	25.7%	14.1%

Additionally, this kind of oxidation process on a-C:H surface is accompanied by the alteration of the mechanical properties which makes the oxide layer more prone to wear, especially under high load [57,58]. As shown in Fig. 8, the wear volumes of a-C:H under low applied load of 1 N (580 MPa, maximum Hertzian contact pressure) kept at low level for the test time ranging from 30 to 140 mins, indicating ZDDP can form effectively anti-wear tribofilms on a-C:H surfaces. However, when increasing the applied load to 10 N (1.2 GPa) and 30 N (1.8 GPa), the coverage of ZDDP tribofilms on coating surface decreased notably (Fig. 8B and C), resulting in significant increase in wear volume. Compared with ZDDP tribofilms formed on ferrous surfaces which show good anti-wear properties even under 5.2 GPa [20,59], the tribofilms formed on a-C:H are less durable under high applied loads due to the easy-shear capability of oxidized a-C:H layer.

3.4. Dominating role of tribofilm in the friction and wear behaviors

It is well accepted that friction and wear behaviors are dominated by tribofilms formed on contact surfaces [60–62]. Gaining fundamental insights into the tribofilm growth mechanism can benefit a better understanding of the tribological mechanisms. Based on above findings, a schematic illustration of tribofilm growth mechanism on a-C:H surfaces is displayed in Fig. 9 and used to clarify the tribological behaviors. As shown in the schematic illustration, when ZDDP is used alone in lubricating oil, tribofilms prefer to form on the steel surface rather than a-C:H. Since the hardness of a-C:H is obviously higher than steel and ZDDP (hardness: a-C:H: 21 GPa > steel: 8 GPa> ZDDP tribofilm: below 3.3 GPa) [63–65], the wear at initial stage mainly happens on steel surface and results in abundant nascent surfaces that is easily oxidized in the tribological process. These oxide areas provide active sites for the tribofilm growth based on Lewis acid-base interaction (Fe^{3+}-Lewis acid, phosphate-Lewis base) [17,18]. Given the Lewis base property of a-C:H, ZDDP tribofilm (Lewis base) prefer to be formed on steel surface rather than a-C:H. After the initial stage, wear mainly takes place on ZDDP tribofilm, considering its significantly low hardness [65]. Then, remarkable wear on steel surface and undetectable wear on a-C:H surface were observed. In addition, since the friction behavior mainly depends on the shear process of ZDDP tribofilms, the friction coefficient is close to the condition of ferrous/ferrous contacts with ZDDP as additive [66].

When adding MoDTC into the above lubricating oil, MoDTC-derived MoO_3 can perform catalytic oxidation action towards a-C:H surface [51–56,67–69], which transforms a-C:H surface from Lewis base to Lewis acid [40,41], providing active growth sites for ZDDP tribofilms. In view of the continuous formation of ZDDP tribofilm on a-C:H surface, slight wear was observed on a-C:H surface. As indicated above, the tribofilms composed of tribochemical products with lower transmittance (e.g., MoS_2) can introduce measurement deviations of Raman-based profilometry in the form of depth rising. Fig. 2 presents the wear profiles obtained by Raman-based method and there is no depth rising, indicating no formation of crystal MoS_2 in the tribofilm. For locating the MoDTC-derived MoS_2, Raman tests were conducted on the steel ball surfaces as shown in Fig. S4. Compared with the test condition with only MoDTC as additive in Fig. S4B, the Raman signal intensity of MoS_2 increases significantly when using MoDTC and ZDDP (Fig. S4A), indicating MoDTC-derived MoS_2 crystals preferred to accumulate and grow into large size on steel surface under the existence of ZDDP. As reported in previous work [8,24,68,70], ZDDP will decompose into small molecular fragments with abundant sulfur atoms which can react with ferrous surfaces to form mixtures of FeS/ZnS. These mixtures provide active S^{2-} to promote the sulfuration of molybdenum oxysulphide into MoS_2 units. These units progressively grow into large lamellar sheets and cover the contact asperities on steel surface, further resulting in low friction. This explains why the friction coefficient kept at low values in the initial stage and decreased with time due to the formation of large MoS_2 sheets.

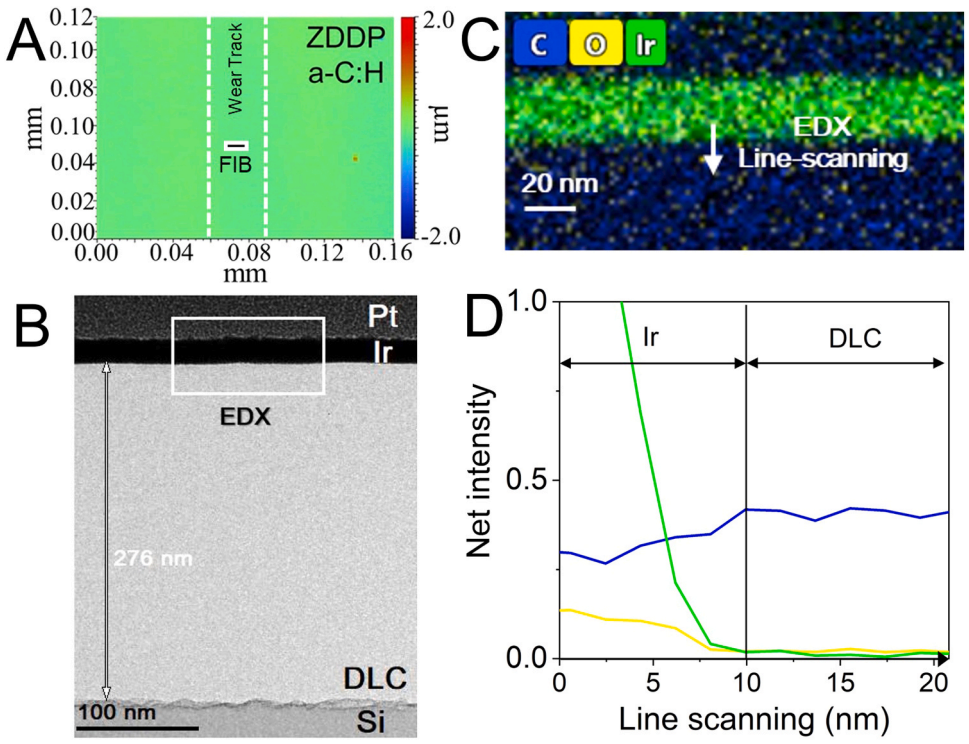

Fig. 7. (A) 3D optical microscopic image of wear scar on DLC coating (PAO4 +0.8 wt% ZDDP) showing the FIB position. (B) TEM image showing the cross-sectional morphology of marked area in Fig. A and EDX mapping position. (C) EDX mapping on the marked area in (B). (D) EDX line-scanning profile along the trace as marked in (C).

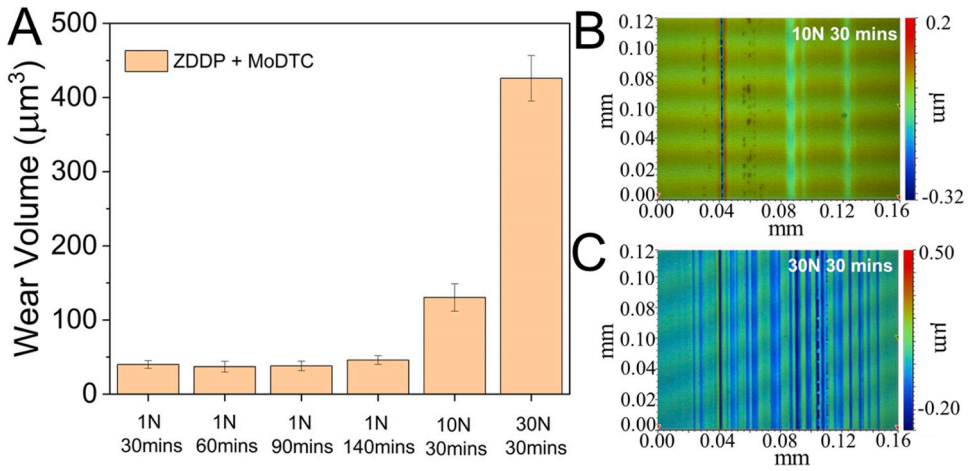

Fig. 8. Wear behaviors of a-C:H in additive-lubricated conditions (PAO + 0.8 wt% ZDDP +0.8 wt% MoDTC) under different time and loads. (A) Wear volumes. (B) 3D optical images under the tribo-test condition of 10 N (1.2 GPa) and 30 mins. (C) 3D optical images under the tribo-test condition of 30 N (1.8 GPa) and 30 mins.

As indicated in the previous study [29,71,72], MoDTC derived tribochemical products can accelerate the wear of DLC, which is attributed to the easy-shear capability of oxidized a-C:H layer caused by MoO_3 in the first stage and the abrasive wear of hard MoC formed via tribo-induced carburization of MoS_2 in the following stage. However, when using ZDDP in combination with MoDTC, the wear acceleration of a-C:H was significantly improved since a protective ZDDP-derived tribofilms are formed on the top of oxidized a-C:H layer. More importantly, the local stress concentration caused by increased surface roughness under severe wear can be obviously alleviated [73–75], which prevent the tribo-induced carburization of MoS_2 into hard MoC particles and the following abrasive wear.

4. Conclusion

Raman-based profilometry was employed to identify the additive-derived tribofilms on a-C:H coatings based on their distinct optical properties. Its effectiveness in in-situ identification is fully demonstrated by combining TEM, EDS, and EELS. The obtained results confirmed the ZDDP-derived tribofilm prefer to form on a-C:H surface when combining MoDTC, due to the catalytic oxidation effect of MoDTC-derived MoO_3 towards the coating surface. This oxidation process can transform a-C:H surface from Lewis base to Lewis acid, providing active growth sites for ZDDP tribofilms. It gives direct evidence that Lewis acid-base interaction plays a crucial in the initial tribochemical reaction (nucleation stage) between ZDDP-derived phosphates and oxidized a-C:H surface

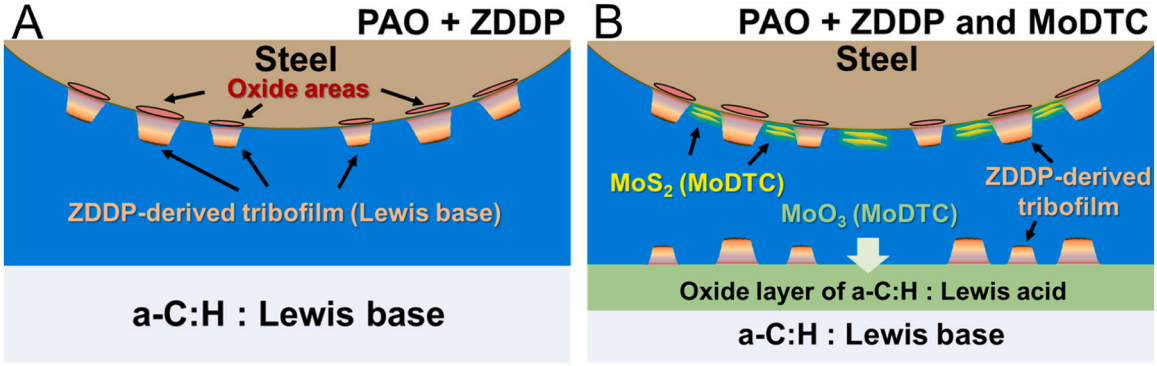

Fig. 9. The tribofilm growth mechanism on a-C:H surface with different additives. (A) ZDDP. (B) ZDDP and MoDTC.

under low applied stress and temperature conditions. In addition, the lower durability of ZDDP tribofilm formed on a-C:H surface is attributed to the easy-shear capability of oxidized a-C:H layer. This Raman-based profilometry propose a new pathway for identifying additive-derived tribofilms formed on coating surfaces which can help gain fundamental insights into tribofilm growth mechanisms, and thus benefit a better understanding of the tribological mechanisms and the development of effective lubricating solutions for diverse surface materials.

Statement of originality

I, the Corresponding Author, declare that this manuscript is original, has not been published before and is not currently being considered for publication elsewhere. I can confirm that the manuscript has been read and approved by all named authors and that there are no other persons who satisfied the criteria for authorship but are not listed. I further confirm that the order of authors listed in the manuscript has been approved by all of us. I understand that the Corresponding Author is the sole contact for the Editorial process and is responsible for communicating with the other authors about progress, submissions of revisions and final approval of proofs.

CRediT authorship contribution statement

Morina Ardian: Writing – review & editing, Supervision, Project administration, Methodology, Funding acquisition, Conceptualization. **Yang Liuquan:** Writing – review & editing, Methodology, Investigation. **Wang Dongze:** Writing – original draft, Methodology, Investigation. **Wang Chun:** Writing – review & editing, Methodology, Investigation. **Xu Nan:** Writing – review & editing, Writing – original draft, Visualization, Validation, Methodology, Investigation, Formal analysis, Data curation, Conceptualization.

Declaration of Competing Interest

The authors declare that they have no known competing financial interests or personal relationships that could have appeared to influence the work reported in this paper.

Data availability

Data will be made available on request.

Acknowledgments

The authors thank the helpful assistance for FIB and TEM tests by Mr. John Harrington, Mrs. Zebeada Aslam, and Mr. Stuart Micklethwaite from Leeds Electron Microscopy and Spectroscopy Centre (LEMAS), University of Leeds. The authors are grateful for facility access support by the Engineering and Physical Sciences Research Council (EPSRC, Grant no. EP/R02524X/1) in the UK. This work is partly supported by the Engineering and Physical Sciences Research Council (grant number EP/R001766/1) as a part of "Friction: The Tribology Enigma" (www.friction.org.uk), a Collaborative Programme Grant between the universities of Leeds and Sheffield.

Appendix A. Supporting information

Supplementary data associated with this article can be found in the online version at doi:10.1016/j.triboint.2024.109335.

References

[1] Holmberg K, Matthews A. Coatings Tribology: Properties, Techniques, and Applications in Surface Engineering. Amsterdam; New York: Elsevier; 2009.
[2] Li Z, Wang Y, Cheng X, Zeng Z, Li J, Lu X, et al. Continuously growing ultrathick CrN coating to achieve high load-bearing capacity and good tribological property. ACS Appl Mater Interfaces 2018;10:2965–75. https://doi.org/10.1021/acsami.7b16426.
[3] Manimunda P, Al-Azizi A, Kim SH, Chromik RR. Shear-induced structural changes and origin of ultralow friction of hydrogenated diamond-like carbon (DLC) in dry environment. ACS Appl Mater Interfaces 2017;9:16704–14. https://doi.org/10.1021/acsami.7b03360.
[4] Härkönen E, Kolev I, Díaz B, Światowska J, Maurice V, Seyeux A, et al. Sealing of hard CrN and DLC coatings with atomic layer deposition. ACS Appl Mater Interfaces 2014;6:1893–901. https://doi.org/10.1021/am404906x.
[5] Fan X, Wang L, Li W, Wan S. Improving tribological properties of multialkylated cyclopentanes under simulated space environment: two feasible approaches. ACS Appl Mater Interfaces 2015;7:14359–68. https://doi.org/10.1021/acsami.5b03088.
[6] Zou YS, Wu YF, Yang H, Cang K, Song GH, Li ZX, et al. The microstructure, mechanical and friction properties of protective diamond like carbon films on magnesium alloy. Appl Surf Sci 2011;258:1624–9. https://doi.org/10.1016/j.apsusc.2011.10.031.
[7] Kosarieh S, Morina A, Lainé E, Flemming J, Neville A. The effect of MoDTC-type friction modifier on the wear performance of a hydrogenated DLC coating. Wear 2013;302:890–8. https://doi.org/10.1016/j.wear.2012.12.052.
[8] Neville A, Morina A, Haque T, Voong M. Compatibility between tribological surfaces and lubricant additives—How friction and wear reduction can be controlled by surface/lube synergies. Tribol Int 2007;40:1680–95. https://doi.org/10.1016/j.triboint.2007.01.019.
[9] Haque T, Morina A, Neville A, Kapadia R, Arrowsmith S. Effect of oil additives on the durability of hydrogenated DLC coating under boundary lubrication conditions. Wear 2009;266:147–57. https://doi.org/10.1016/j.wear.2008.06.011.
[10] Mistry KK, Morina A, Neville A. A tribochemical evaluation of a WC–DLC coating in EP lubrication conditions. Wear 2011;271:1739–44. https://doi.org/10.1016/j.wear.2011.01.071.
[11] Haque T, Morina A, Neville A, Kapadia R, Arrowsmith S. Non-ferrous coating/lubricant interactions in tribological contacts: assessment of tribofilms. Tribol Int 2007;40:1603–12. https://doi.org/10.1016/j.triboint.2007.01.023.
[12] De Feo M, De Barros Bouchet MI, Minfray C, Esnouf C, Le Mogne Th, Meunier F, et al. Formation of interfacial molybdenum carbide for DLC lubricated by MoDTC: origin of wear mechanism. Wear 2017;370–371:17–28. https://doi.org/10.1016/j.wear.2016.10.002.
[13] De Feo M, De Barros Bouchet MI, Minfray C, Le Mogne Th, Meunier F, Yang L, et al. MoDTC lubrication of DLC-involving contacts. Impact of MoDTC degradation. Wear 2016;348–349:116–25. https://doi.org/10.1016/j.wear.2015.12.001.
[14] Okubo H, Sasaki S. In situ Raman observation of structural transformation of diamond-like carbon films lubricated with MoDTC solution: mechanism of wear

acceleration of DLC films lubricated with MoDTC solution. Tribol Int 2017;113:399–410. https://doi.org/10.1016/j.triboint.2016.10.009.
[15] Okubo H, Tadokoro C, Sumi T, Tanaka N, Sasaki S. Wear acceleration mechanism of diamond-like carbon (DLC) films lubricated with MoDTC solution: roles of tribofilm formation and structural transformation in wear acceleration of DLC films lubricated with MoDTC solution. Tribol Int 2019;133:271–87. https://doi.org/10.1016/j.triboint.2018.12.029.
[16] Gosvami NN, Bares JA, Mangolini F, Konicek AR, Yablon DG, Carpick RW. Mechanisms of antiwear tribofilm growth revealed in situ by single-asperity sliding contacts. Science 2015;348:102–6. https://doi.org/10.1126/science.1258788.
[17] Martin JM, Onodera T, Minfray C, Dassenoy F, Miyamoto A. The origin of anti-wear chemistry of ZDDP. Faraday Discuss 2012;156:311. https://doi.org/10.1039/c2fd00126h.
[18] Spikes H. The history and mechanisms of ZDDP. Tribol Lett 2004;17:469–89. https://doi.org/10.1023/B:TRIL.0000044495.26882.b5.
[19] Salinas Ruiz VR, Kuwahara T, Galipaud J, Masenelli-Varlot K, Hassine MB, Héau C, et al. Interplay of mechanics and chemistry governs wear of diamond-like carbon coatings interacting with ZDDP-additivated lubricants. Nat Commun 2021;12:4550. https://doi.org/10.1038/s41467-021-24766-6.
[20] Vengudusamy B, Green JH, Lamb GD, Spikes HA. Durability of ZDDP tribofilms formed in DLC/DLC contacts. Tribol Lett 2013;51:469–78. https://doi.org/10.1007/s11249-013-0185-z.
[21] Ueda M, Kadiric A, Spikes H. ZDDP tribofilm formation on non-ferrous surfaces. Tribology 2020;15:318–31. https://doi.org/10.2474/trol.15.318.
[22] Haque T, Morina A, Neville A. Influence of friction modifier and antiwear additives on the tribological performance of a non-hydrogenated DLC coating. Surf Coat Technol 2010;204:4001–11. https://doi.org/10.1016/j.surfcoat.2010.05.017.
[23] Vengudusamy B, Green JH, Lamb GD, Spikes HA. Tribological properties of tribofilms formed from ZDDP in DLC/DLC and DLC/steel contacts. Tribol Int 2011;44:165–74. https://doi.org/10.1016/j.triboint.2010.10.023.
[24] Martin J, Grossiord C, Varlot K, Vacher B, Igarashi J. Synergistic effects in binary systems of lubricant additives: a chemical hardness approach. Tribol Lett 2000;8:193–201. https://doi.org/10.1023/A:1019147520893.
[25] Minfray C, Martin JM, Barros MID, Mogne TL, Kersting R, Hagenhoff B. Chemistry of ZDDP tribofilm by ToF-SIMS. Tribol Lett 2004;17:351–7. https://doi.org/10.1023/B:TRIL.0000044483.68571.49.
[26] Onodera T, Martin JM, Minfray C, Dassenoy F, Miyamoto A. Antiwear chemistry of ZDDP: coupling classical MD and tight-binding quantum chemical MD methods (TB-QCMD). Tribol Lett 2013;50:31–9. https://doi.org/10.1007/s11249-012-0063-0.
[27] Martin JM. Antiwear mechanisms of zinc dithiophosphate: a chemical hardness approach. Tribol Lett 1999;6:1–8. https://doi.org/10.1023/A:1019191019134.
[28] Xu N, Wang C, Yang L, Barimah EK, Jose G, Neville A, et al. Nano-scale coating wear measurement by introducing Raman-sensing underlayer. J Mater Sci Technol 2022;96:285–94. https://doi.org/10.1016/j.jmst.2021.04.031.
[29] Xu N, Wang C, Yang L, Jose G, Morina A. Probing the tribochemical impact on wear rate dynamics of hydrogenated amorphous carbon via raman-based profilometry. ACS Appl Mater Interfaces 2022;14:2071–81. https://doi.org/10.1021/acsami.1c21824.
[30] Wang P, He Q, Lu M, Li W, Peng B. Evolutionary mechanism of the defects in the fluoride-containing phosphate based glasses induced by gamma radiation. Sci Rep 2016;6:18926. https://doi.org/10.1038/srep18926.
[31] Lin F, Mao S, Meng Z, Zeng H, Qiu J, Yue Y, et al. Fullerene doped glasses. Appl Phys Lett 1994;65:2522–4. https://doi.org/10.1063/1.112623.
[32] Ghosh A, Sadeghi F. A novel approach to model effects of surface roughness parameters on wear. Wear 2015;338–339:73–94. https://doi.org/10.1016/j.wear.2015.04.022.
[33] Hisakado T. Effect of surface roughness on contact between solid surfaces. Wear 1974;28:217–34. https://doi.org/10.1016/0043-1648(74)90163-X.
[34] Jiang J, Arnell RD. The effect of substrate surface roughness on the wear of DLC coatings. Wear 2000;239:1–9. https://doi.org/10.1016/S0043-1648(99)00351-8.
[35] Mangolini F, Li Z, Marcus MA, Schneider R, Dienwiebel M. Quantification of the carbon bonding state in amorphous carbon materials: a comparison between EELS and NEXAFS measurements. Carbon 2021;173:557–64. https://doi.org/10.1016/j.carbon.2020.11.021.
[36] Jäger C, Henning Th, Schlögl R, Spillecke O. Spectral properties of carbon black. J Non-Cryst Solids 1999;258:161–79. https://doi.org/10.1016/S0022-3093(99)00436-6.
[37] Chen X, Zhang C, Kato T, Yang X, Wu S, Wang R, et al. Evolution of tribo-induced interfacial nanostructures governing superlubricity in a-C:H and a-C:H:Si films. Nat Commun 2017;8:1675. https://doi.org/10.1038/s41467-017-01717-8.
[38] Zhang X, Schneider R, Müller E, Gerthsen D. Practical aspects of the quantification of sp2-hybridized carbon atoms in diamond-like carbon by electron energy loss spectroscopy. Carbon 2016;102:198–207. https://doi.org/10.1016/j.carbon.2016.02.020.
[39] Bruley J, Madakson P, Liu JC. Characterization of CVD-hydrogenated diamondlike thin films on silicon by EELS, RBS/channeling and nuclear reaction analysis. Nucl Instrum Methods Phys Res Sect B Beam Interact Mater At 1990;45:618–21. https://doi.org/10.1016/0168-583X(90)90912-E.
[40] Zong E, Wei D, Wan H, Zheng S, Xu Z, Zhu D. Adsorptive removal of phosphate ions from aqueous solution using zirconia-functionalized graphite oxide. Chem Eng J 2013;221:193–203. https://doi.org/10.1016/j.cej.2013.01.088.
[41] Dreyer DR, Jarvis KA, Ferreira PJ, Bielawski CW. Graphite oxide as a carbocatalyst for the preparation of fullerene-reinforced polyester and polyamide nanocomposites. Polym Chem 2012;3:757. https://doi.org/10.1039/c2py00545j.
[42] Zeng S, Liu L, Shang D, Feng J, Dong H, Xu Q, et al. Efficient and reversible absorption of ammonia by cobalt ionic liquids through Lewis acid–base and cooperative hydrogen bond interactions. Green Chem 2018;20:2075–83. https://doi.org/10.1039/C8GC00215K.
[43] Ji J, Xiong W, Zhang X, Peng L, Shi M, Wu Y, et al. Reversible absorption of NF3 with high solubility in Lewis acidic ionic liquids. Chem Eng J 2022;440:135902. https://doi.org/10.1016/j.cej.2022.135902.
[44] Lu W, Yuan M, Chen J, Zhang J, Kong L, Feng Z, et al. Synergistic Lewis acid-base sites of ultrathin porous Co3O4 nanosheets with enhanced peroxidase-like activity. Nano Res 2021;14:3514–22. https://doi.org/10.1007/s12274-021-3656-9.
[45] Frank B, Blume R, Rinaldi A, Trunschke A, Schlögl R. Oxygen insertion catalysis by sp2 carbon. Angew Chem Int Ed 2011;50:10226–30. https://doi.org/10.1002/anie.201103340.
[46] Gao Y, Tang P, Zhou H, Zhang W, Yang H, Yan N, et al. Graphene oxide catalyzed C−H bond activation: the importance of oxygen functional groups for biaryl construction. Angew Chem Int Ed 2016;55:3124–8. https://doi.org/10.1002/anie.201510081.
[47] Yu Q, Chen X, Zhang C, Xu J, Qi W, Deng W, et al. Influencing mechanisms of deposition bias voltage on superlubricious a-C:H films: key role of nanoclustering structures in controlling structural evolution of transfer film. Carbon 2022;196:499–509. https://doi.org/10.1016/j.carbon.2022.05.014.
[48] Wang K, Zhang J, Ma T, Liu Y, Song A, Chen X, et al. Unraveling the friction evolution mechanism of diamond-like carbon film during nanoscale running-in process toward superlubricity. Small 2021;17:2005607. https://doi.org/10.1002/smll.202005607.
[49] Kassim KAM, Tokoroyama T, Murashima M, Umehara N. The wear classification of MoDTC-derived particles on silicon and hydrogenated diamond-like carbon at room temperature. Tribol Int 2020;147:106176. https://doi.org/10.1016/j.triboint.2020.106176.
[50] Yoshida Y, Kunitsugu S. Friction wear characteristics of diamond-like carbon coatings in oils containing molybdenum dialkyldithiocarbamate additive. Wear 2018;414–415:118–25. https://doi.org/10.1016/j.wear.2018.08.004.
[51] Afsharpour M, Mahjoub A, Amini MM. A nano-hybrid of molybdenum oxide intercalated by dithiocarbamate as an oxidation catalyst. J Inorg Organomet Polym 2008;18:472–6. https://doi.org/10.1007/s10904-008-9223-y.
[52] Liu S, Obuchi A, Uchisawa J, Nanba T, Kushiyama S. An exploratory study of diesel soot oxidation with NO2 and O2 on supported metal oxide catalysts. Appl Catal B Environ 2002;37:309–19. https://doi.org/10.1016/S0926-3373(02)00008-5.
[53] Neeft JPA, Makkee M, Moulijn JA. Metal oxides as catalysts for the oxidation of soot. Chem Eng J Biochem Eng J 1996;64:295–302. https://doi.org/10.1016/S0923-0467(96)03138-7.
[54] Jelles SJ, Van Setten BAAL, Makkee M, Moulijn JA. Molten salts as promising catalysts for oxidation of diesel soot: importance of experimental conditions in testing procedures. Appl Catal B Environ 1999;21:35–49. https://doi.org/10.1016/S0926-3373(99)00011-9.
[55] Liu S, Obuchi A, Oi-Uchisawa J, Nanba T, Kushiyama S. Synergistic catalysis of carbon black oxidation by Pt with MoO3 or V2O5. Appl Catal B Environ 2001;30:259–65. https://doi.org/10.1016/S0926-3373(00)00238-1.
[56] Toniolo FS, Barbosa-Coutinho E, Schwaab M, Leocadio ICL, Aderne RS, Schmal M, et al. Kinetics of the catalytic combustion of diesel soot with MoO3/Al2O3 catalyst from thermogravimetric analyses. Appl Catal A Gen 2008;342:87–92. https://doi.org/10.1016/j.apcata.2008.03.004.
[57] Wang D-Y, Chang C-L, Ho W-Y. Oxidation behavior of diamond-like carbon films. 138–44 Surf Coat Technol 1999;120–121. https://doi.org/10.1016/S0257-8972(99)00350-3.
[58] Alazizi A, Draskovics A, Ramirez G, Erdemir A, Kim SH. Tribochemistry of carbon films in oxygen and humid environments: oxidative wear and galvanic corrosion. Langmuir 2016;32:1996–2004. https://doi.org/10.1021/acs.langmuir.5b04207.
[59] Equey S, Roos S, Mueller U, Hauert R, Spencer ND, Crockett R. Reactions of zinc-free anti-wear additives in DLC/DLC and steel/steel contacts. Tribol Int 2008;41:1090–6. https://doi.org/10.1016/j.triboint.2008.03.004.
[60] Morina A, Zhao H, Mosselmans JFW. In-situ reflection-XANES study of ZDDP and MoDTC lubricant films formed on steel and diamond like carbon (DLC) surfaces. Appl Surf Sci 2014;297:167–75. https://doi.org/10.1016/j.apsusc.2014.01.116.
[61] Erdemir A, Ramirez G, Eryilmaz OL, Narayanan B, Liao Y, Kamath G, et al. Carbon-based tribofilms from lubricating oils. Nature 2016;536:67–71. https://doi.org/10.1038/nature18948.
[62] Wu H, Khan AM, Johnson B, Sasikumar K, Chung Y-W, Wang QJ. Formation and nature of carbon-containing tribofilms. ACS Appl Mater Interfaces 2019;11:16139–46. https://doi.org/10.1021/acsami.8b22496.
[63] Ward L, Junge F, Lampka A, Dobbertin M, Mewes C, Wienecke M. The effect of bias voltage and gas pressure on the structure, adhesion and wear behavior of diamond like carbon (DLC) coatings with Si interlayers. Coatings 2014;4:214–30. https://doi.org/10.3390/coatings4020214.
[64] Fang L, Korres S, Lamberti WA, Webster MN, Carpick RW. What stress components drive mechanochemistry? A study of ZDDP tribofilm formation. Faraday Discuss 2023;241:394–412. https://doi.org/10.1039/D2FD00123C.
[65] Ueda M, Kadiric A, Spikes H. On the crystallinity and durability of ZDDP tribofilm. Tribol Lett 2019;67:123. https://doi.org/10.1007/s11249-019-1236-x.
[66] Taylor LJ, Spikes HA. Friction-enhancing properties of ZDDP antiwear additive: part I—friction and morphology of ZDDP reaction films. Tribol Trans 2003;46:303–9. https://doi.org/10.1080/10402000308982630.
[67] Akbari S, Kovač J, Kalin M. Effect of ZDDP concentration on the thermal film formation on steel, hydrogenated non-doped and Si-doped DLC. Appl Surf Sci 2016;383:191–9. https://doi.org/10.1016/j.apsusc.2016.04.182.

[68] Cyriac F, Yi TX, Poornachary SK, Chow PS. Behavior and interaction of boundary lubricating additives on steel and DLC-coated steel surfaces. Tribol Int 2021;164:107199. https://doi.org/10.1016/j.triboint.2021.107199.
[69] Okubo H, Watanabe S, Tadokoro C, Sasaki S. Effects of structure of zinc dialkyldithiophosphates on tribological properties of tetrahedral amorphous carbon film under boundary lubrication. Tribol Int 2016;98:26–40. https://doi.org/10.1016/j.triboint.2016.02.025.
[70] De Barros'Bouchet MI, Martin JM, Le-Mogne T, Vacher B. Boundary lubrication mechanisms of carbon coatings by MoDTC and ZDDP additives. Tribol Int 2005;38:257–64. https://doi.org/10.1016/j.triboint.2004.08.009.
[71] Espejo C, Thiébaut B, Jarnias F, Wang C, Neville A, Morina A. MoDTC tribochemistry in steel/steel and steel/diamond-like-carbon systems lubricated with model lubricants and fully formulated engine oils. J Tribol 2019;141:012301. https://doi.org/10.1115/1.4041017.
[72] Kassim KAM, Tokoroyama T, Murashima M, Lee W-Y, Umehara N, Mustafa MMB. Wear acceleration of a-C:H coatings by molybdenum-derived particles: Mixing and temperature effects. Tribol Int 2021;159:106944. https://doi.org/10.1016/j.triboint.2021.106944.
[73] Arola D, Williams C. Estimating the fatigue stress concentration factor of machined surfaces. Int J Fatigue 2002;24:923–30. https://doi.org/10.1016/S0142-1123(02)00012-9.
[74] Leiro A, Kankanala A, Vuorinen E, Prakash B. Tribological behaviour of carbide-free bainitic steel under dry rolling/sliding conditions. Wear 2011;273:2–8. https://doi.org/10.1016/j.wear.2011.03.025.
[75] Teles VC, De Mello JDB, Da Silva WM. Abrasive wear of multilayered/gradient CrAlSiN PVD coatings: effect of interface roughness and of superficial flaws. 1691–701 Wear 2017;376–377. https://doi.org/10.1016/j.wear.2017.01.116.